Electro-osmotic dispersion in a circular tube with slip-stick striped wall

Qi Zhou*, Chiu-On Ng

Department of Mechanical Engineering, The University of Hong Kong

Pokfulam Road, Hong Kong

Abstract

The hydrodynamic dispersion of a neutral non-reacting solute due to steady electro-osmotic flow (EOF) in a circular channel with longitudinal step changes of zeta potential and hydrodynamic slippage is analyzed in this study. The channel wall is periodically micro-patterned along the axial position with alternating slip-stick stripes of distinct zeta potentials. Existing studies on electrically driven hydrodynamic dispersion are based on flow subject to either the no-slip boundary condition on the capillary surface or the simplification of lubrication approximation. Taking wall slippage into account, a homogenization analysis is performed in this study to derive the hydrodynamic dispersion coefficient without subject to the long-wave constraint of the lubrication approximation, but for a general case where the length of one periodic unit of wall pattern is comparable with the channel radius. The flow and the hydrodynamic dispersion coefficient are calculated numerically, using the packages MATLAB and COMSOL, as functions of controlling parameters including the period length of the wall pattern, the area fraction of the slipping region (EOF-suppressing) in a periodic unit, the ratio of the two zeta potentials, the intrinsic hydrodynamic slip length, the Debye parameter, and the Péclet number. The dispersion is found to show notable, non-monotonic in certain situations, dependence on these controlling parameters. It is noteworthy that the introduction of hydrodynamic slippage will generate much richer behaviors of the hydrodynamic dispersion than the situation with no-slip boundary condition, as slippage interacts with zeta potentials in the EOF-suppressing and EOF-supporting regions.

Keywords: *electro-osmotic flow, slippage, hydrodynamic dispersion, plate height, homogenization analysis*

*Corresponding author: lycezqwd@gmail.com
Qi Zhou is currently with Department of Mechanical and Automation Engineering, The Chinese University of Hong Kong, Shatin, NT, Hong Kong

1. Introduction

In contrast with pressure-driven flow, which is characterized with a parabolic velocity profile and usually leads to significant dispersion, typical electro-osmotic flow (EOF) has a plug-like velocity profile in the thin electric double layer (EDL) limit and generates much weaker dispersion. Dispersion is known to be conducive for mixing but detrimental for separation in microfluidic applications. Therefore, EOF is more desirable for separation processes and widely employed in capillary zone electrophoresis (CZE) and capillary electrochromatography (CEC), for both of which the resolution is limited by band-broadening of the analytes due to dispersion (Ghosal 2006). In terms of theoretical research, one of the earliest studies on dispersion in EOF was pioneered by Martin and Guiochon (1984), who analyzed the zone broadening resulting from EOF and the retention in open-tubular capillary liquid chromatography based on an approximated EO velocity. Subsequently, many other authors (Datta and Kotamarthi 1990, Griffiths and Nilson 1999, 2000, Zholkovskij *et al* 2003, Zholkovskij and Masliyah 2004, Paul and Ng 2012a, b, etc.) studied the hydrodynamic dispersion arising from either pure EOF or EOF incorporated with pressure-driven flow. A comprehensive review on this topic was given by Datta and Ghosal (2009).

Surface heterogeneity (e.g. surface topography, charge distribution, slippage modulation, etc.), which may occur naturally or be engineered artificially, can lead to opposite effects on the dispersion depending on whether the flow is driven by pressure or electric field. Generally speaking, with the introduction of surface heterogeneities on the channel wall, dispersion is inhibited for pressure-driven flow, but enhanced for EOF. For pressure-driven flow, the dominant effect caused by these surface non-uniformities on the dispersion is attributed to the transverse or secondary flows generated in the vicinity of the discontinuities (Ajdari 1996), which will contribute to cross-sectional mixing and therefore reduce the axial dispersion (Stroock and Whitesides 2003, Zhao and Bau 2007). For EOF, the dominant effect is by the pressure gradients locally induced to maintain flow continuity (otherwise violated due to the discontinuities on the heterogeneous surface). The plug-like velocity profile of the EOF will be distorted by the superimposed parabolic velocity of the induced pressure-driven flow and altered into a velocity profile of larger gradient, leading to enhanced dispersion.

On employing numerical simulations, Potoćek *et al* (1995) showed that the plug-like EOF would fail to materialize and significant dispersion of sample peaks would happen when the zeta potential is longitudinally inhomogeneous. Previously, Anderson and Idol (1985) had developed an infinite-series solution for electro-osmotic flow through a charged capillary with an arbitrary axial distribution of zeta potential. Effects of flow perturbations due to charge non-uniformities (denoted as *surface defects* in their paper) on the dispersion in capillary electrophoresis were then analytically examined by Long *et al* (1999). In their problem, pressure jumps were induced by the presence of surface defects, resulting in possible occurrence of recirculating flows. They showed that a localized defect, from which the velocity perturbation decays only algebraically, could cause hydrodynamic dispersion over a long distance. The same problem was investigated both analytically and experimentally by Herr *et al* (2000), who considered discrete step changes in zeta potential (EOF-suppressing region and EOF-supporting region) distributed at

various distances along a cylindrical capillary. They provided empirical evidence to demonstrate that dispersion in the EOF-supporting region increases as the area fraction of the EOF-suppressing region increases. More recent studies on the non-uniformity of wall potential causing increased dispersion involve Ghosal (2002a, 2002b, 2003), Zholkovskij *et al* (2010) and so on.

All studies mentioned above on the dispersion due to EOF, however, are based on flows subject to the assumption of no-slip boundary condition, which may not be valid for microfluidic flows. In microfluidics, the channel wall is an essential issue and has crucial influence on the flow morphology and mass transport. It can either be naturally micro-/nanostructured or deliberately treated to become hydrophobic or even superhydrophobic, resulting in a low-viscosity or depletion layer that lubricates the flow over the surface and thus amounting to boundary slip. It has been well accepted that even a small amount of boundary slip can substantially enhance EOF since the first relevant analysis by Muller *et al* (1986). Squires (2008) developed some general rules of electrokinetic flows over slipping surfaces exhibiting heterogeneous distributions of zeta potential and slip length in the thin EDL limit. EOF over an anisotropic superhydrophobic surface that is inhomogeneously charged and slipping was further studied by Belyaev and Vinogradova (2011), who revealed relations between the EO mobility and hydrodynamic slip under the conditions of a very thick channel and a very thin EDL. The relations were then generalized by Ng and Chu (2011), who derived the Onsager relations applicable to arbitrary channel and EDL thickness for electro-hydrodynamic flows through a planar channel made up of stripe-patterned superhydrophobic surfaces. Some other studies on EOF addressing surface heterogeneities were conducted by Bahga et al (2010), Zhao (2010, 2011), Ng and Zhou (2012a), Zhao and Yang (2012), Chu and Ng (2012) and Datta and Choudhary (2013). Refer to Rothstein (2010) for a recent review of slip on superhydrophobic surfaces.

Given that EOF can be sensitively affected by boundary slip, it is of interest to look into how dispersion in EOF can be affected by the slip. Previously, we (Ng and Zhou 2012b) have performed an analytical study on dispersion arising from EOF in a circular microchannel with longitudinal non-uniformities of wall potential and hydrodynamic slippage, in which we demonstrated how the presence of slip can dramatically change the effect of the non-uniform wall potential on the dispersion. It was shown that the non-uniform wall potential, interacting with non-uniform slip, leads to effects more intensive than the situation when the wall potential and slip are both uniform with a value equivalent to the system average of the non-uniform distribution. The study could be straightforwardly generalized to typical slip-stick patterns as step changes of zeta potential and hydrodynamic slippage (see Appendix). However, since the analysis was based on lubrication approximation assuming slowly varying wall pattern and unidirectional flow, the transverse flow as well as its associated mixing effect near the discontinuity was ignored. Therefore, it could at best provide qualitative features of the long-range perturbation due to surface heterogeneities on the dispersion. Its quantitative accuracy, which could be low given the validation of lubrication theory for a geometry involving step changes, is subject to scrutiny. This has motivated the present study, which abandons the lubrication approximation and considers a general case where the length scale for variations in the axial direction is comparable with the cross-sectional dimension of the channel.

Specifically, the present problem is concerned about the hydrodynamic dispersion of a non-reacting neutral solute due to steady electro-osmotic flow in a circular capillary with axial step changes of zeta potential and hydrodynamic slippage without subject to lubrication approximation. The flow we consider is one of those studied by Chu and Ng (2012), an electrohydrodynamic flow through a circular tube periodically micro-patterned along the axial position with alternating slip-stick stripes of distinct zeta potentials. The reason why we consider EOF in such geometry is that the stepwise wall pattern may be more realistic and practical to design and fabricate than those slowly and mildly varying patterns for application in microfluidic devices. In the present study, formulation of the EOF is based on Chu and Ng (2012). Expression for the effective dispersion coefficient is derived through a multi-scale asymptotic analysis. Numerical results of the dispersion coefficient are then obtained using the packages MATLAB and COMSOL. Our primary objective is to investigate in a general case how the hydrodynamic dispersion arising from EOF will be affected by the combined effects of non-uniform wall potential and slippage, which in turn can provide us with strategies to suppress or enhance dispersion as needed in lab conditions. We also look into accuracy of the commonly adopted lubrication approximation in estimating the dispersion by comparing our numerical results of the general case with theoretical limits obtained by the lubrication theory.

The experimental setup for detection of solute dispersion in EOF subject to surface heterogeneity was introduced by Herr *et al* (2000). To realize the step change of zeta potential, an EOF-suppressing polymer was adsorbed onto a certain fraction of the transparent fused-silica capillary (forming an opaque polyimide coating), by which they produced a coupled capillary consisting of a coated region with a suppressed zeta potential and a bare region with a normal zeta potential (referred to as *EOF-supporting region*). Imaging was conducted directly on the transparent EOF-supporting region and through pre-manufactured "windows" on the opaque EOF-suppressing region. The information of sample dispersion was optically extracted using the caged-fluorescence technique. Refer to the book chapter by Devasenathipathy and Santiago (2005) for a more detailed introduction of micro-/nanoscale electrokinetic flow diagnostic techniques. For our problem, similar procedures used by Herr *et al* (2000) can be taken to implement experiments, except that step changes of zeta potential and slip length need to be synthesized on the capillary, which may be challenging. Up to now, techniques for the design and fabrication of patterned superhydrophobic surfaces are rather mature (Celia *et al* 2013). Also, with the addition of embedded nanoelectrodes (Dawson and O'Riordan 2014) within the channel wall, the contradiction between a practical slip length and a net charge density at the slip interface (Huang *et al* 2008) can be overcome. The scenario addressing surface characteristics and other practical issues for potential experiment conduction was presented by Steffes *et al* (2011) and Schönecker and Hardt (2014). Promisingly, given all mentioned above, the proposed strategies in the present study for mass transport in electro-osmotic flow may be verified experimentally.

2. Problem formulation

2.1 Electric potential in the EDL

The problem considers dispersion in steady electro-osmotic flow of an incompressible Newtonian fluid through a circular tube, the wall ($r = R$) of which is patterned with a periodic array of alternating slipping and non-slipping stripes of different wall potentials (figure 1(a)). One unit of the wall pattern is of a period length $2l$, consisting of a slipping stripe of $2al$ with slip length λ and zeta potential ζ_S , and a non-slipping strip of $2(1-a)l$ with zeta potential ζ_{NS}. The area fraction a ranges from 0 to 1, denoting proportion of the slipping region. The intrinsic/microscopic slip length λ (Navier's slip length, figure 2) is in the range $0 \sim \infty$, with $\lambda = 0$ corresponding to no-slip and $\lambda = \infty$ corresponding to perfect-slip.

The flow is driven by an external electric field E_z applied in the axial direction. On assuming low potentials (e.g. <25 mV) within a non-overlapped EDL, the Debye-Hückel approximation applies and the electric potential $\psi(r,z)$ of the EDL is expressible by the linearized P-B equation:

$$\nabla^2\psi = \kappa^2\psi \tag{1}$$

where $\kappa = \sqrt{2n_0e^2z_0/\varepsilon k_BT}$ is the Debye-Hückel parameter, or the inverse of the Debye length κ^{-1} (a measure of the EDL thickness). Herein, n_0 is the bulk concentration of the ions at the neutral state, e the elementary charge, z_0 the valence of the ($z_0 : z_0$) symmetrical electrolyte, ε the dielectric constant of the fluid, k_B the Boltzmann constant, and T the absolute temperature. The Debye-Hückel approximation is valid for $z_0e\psi/k_BT < 1$, which physically means that the electric potential is small compared to the thermal potential.

The solution to equation (1) is expressed by:

$$\psi(r,z) = D_0\frac{I_0(\kappa r)}{I_0(\kappa R)} + \sum_{n=1}^{\infty} D_n\cos(\alpha_n z)\frac{I_0(\beta_n r)}{I_0(\beta_n R)} \tag{2}$$

where $\alpha_n = n\pi/L$, $\beta_n^2 = \alpha_n^2 + \kappa^2$, and I_n is the modified Bessel function of the first kind of order n . $D_{0,1,2\ldots n}$ are Fourier series coefficients determined by applying the mixed electric boundary conditions:

$$\psi(R,z) = D_0 + \sum_{n=1}^{\infty} D_n\cos(\alpha_n z) = \begin{cases} \zeta_S & 0 < z < al \\ \zeta_{NS} & al < z < l \end{cases} \tag{3}$$

which are readily found to be:

$$D_0 = a\zeta_S + (1-a)\zeta_{NS}, \quad D_n = 2(\zeta_S - \zeta_{NS})\frac{\sin(na\pi)}{n\pi} \tag{4}$$

On introducing the following normalization:

$$(\hat{r},\hat{z},\hat{\lambda},\hat{l}) = (r,z,\lambda,l)/R, \quad \hat{\kappa} = \kappa R, \quad (\hat{\psi},\hat{\zeta}_S,\hat{D}_0,\hat{D}_n) = (\psi,\zeta,D_0,D_n)/\zeta_{NS} \tag{5}$$

equations (3) and (4) are cast in the dimensionless forms:

$$\hat{D}_0 + \sum_{n=1}^{\infty} \hat{D}_n \cos(\hat{\alpha}_n \hat{z}) = \begin{cases} \hat{\zeta}_S & 0 < z < a\hat{l} \\ 1 & a\hat{l} < z < \hat{l} \end{cases} \tag{6}$$

$$\hat{D}_0 = a\hat{\zeta}_S + 1 - a, \quad \hat{D}_n = 2(\hat{\zeta}_S - 1)\frac{\sin(na\pi)}{n\pi} \tag{7}$$

2.2 Electro-osmotic flow

Given the small dimensions consider in our problem, the flow falls into the low Reynolds number regime, where the Stokes equation is applicable. The governing equation is solved semi-analytically by employing the method of eigenfunction expansion, wherein the coefficients are determined by point collocation. To be specific, the mixed electro-hydrodynamic boundary conditions are implemented by respective point-matching using adequate data points on the two distinct regions within a period length, and the transition of the step change is retained by setting an infinitesimal region to avoid numerical singularity.

The momentum equation is given by:

$$\mu\nabla^2\vec{u} - \nabla p + \rho_e\vec{E} = 0 \tag{8}$$

where $\vec{u} = (u, w)$ is the electro-osmotic velocity and $p(r, z)$ is the locally induced pressure. The charge density $\rho_e(r, z)$ and the total electric field strength $\vec{E}(r, z)$ are expressed by:

$$\rho_e(r, z) = -\varepsilon\nabla^2\psi = -\varepsilon\kappa\psi \tag{9}$$

$$\vec{E}(r, z) = -\nabla\psi + (0, E_z) \tag{10}$$

We adopt the radial and axial velocity components solved by Chu and Ng (2012) as below, where normalizations as in equation (5) have been used:

$$\begin{aligned} u(\hat{r}, \hat{z}) = -\Bigg\{ & \sum_{n=1}^{M} \hat{D}_n \sin(\hat{\alpha}_n \hat{z}) \frac{\hat{\alpha}_n}{\hat{\beta}_n(1 - \hat{\alpha}_n^2/\hat{\beta}_n^2)} \times \left[\frac{I_1(\hat{\beta}_n\hat{r})}{I_0(\hat{\beta}_n)} - \hat{r}\frac{I_1(\hat{\beta}_n)}{I_0(\hat{\beta}_n)}\frac{I_0(\hat{\alpha}_n\hat{r})}{I_0(\hat{\alpha}_n)} \right] \\ & + \sum_{n=1}^{M} \hat{G}_n \sin(\hat{\alpha}_n \hat{z}) \left[\frac{I_1(\hat{\alpha}_n\hat{r})}{I_0(\hat{\alpha}_n)} - \hat{r}\frac{I_1(\hat{\alpha}_n)}{I_0(\hat{\alpha}_n)}\frac{I_0(\hat{\alpha}_n\hat{r})}{I_0(\hat{\alpha}_n)} \right] \Bigg\} E_z^* \end{aligned} \tag{11}$$

$$\begin{aligned} w(\hat{r}, \hat{z}) = -\Bigg\{ & \hat{D}_0 \frac{I_0(\hat{\kappa}\hat{r})}{I_0(\hat{\kappa})} + \hat{G}_0 + \sum_{n=1}^{M} \hat{D}_n \cos(\hat{\alpha}_n \hat{z}) \frac{1}{(1 - \hat{\alpha}_n^2/\hat{\beta}_n^2)} \\ & \times \left[\frac{I_0(\hat{\beta}_n\hat{r})}{I_0(\hat{\beta}_n)} - \frac{I_1(\hat{\beta}_n)}{\hat{\beta}_n I_0(\hat{\beta}_n)} \left(2\frac{I_0(\hat{\alpha}_n\hat{r})}{I_0(\hat{\alpha}_n)} + \hat{\alpha}_n\hat{r}\frac{I_1(\hat{\alpha}_n\hat{r})}{I_0(\hat{\alpha}_n)} \right) \right] \\ & + \sum_{n=1}^{M} \hat{G}_n \cos(\hat{\alpha}_n \hat{z}) \left[\left(1 - \frac{2}{\hat{\alpha}_n}\frac{I_1(\hat{\alpha}_n)}{I_0(\hat{\alpha}_n)} \right) \frac{I_0(\hat{\alpha}_n\hat{r})}{I_0(\hat{\alpha}_n)} - \hat{r}\frac{I_1(\hat{\alpha}_n)}{I_0(\hat{\alpha}_n)}\frac{I_1(\hat{\alpha}_n\hat{r})}{I_0(\hat{\alpha}_n)} \right] \Bigg\} E_z^* \end{aligned} \tag{12}$$

where $E_z^* = -(\varepsilon\hat{\zeta}_{NS}/\mu)E_z$ denotes the Helmholtz-Smoluchowski velocity characteristic of EOF through a homogeneous channel with a very thin EDL. Herein, $-(\varepsilon\hat{\zeta}_{NS}/\mu)$ is the EO mobility and can be

interpreted as another form of "slip" on the interface of the EDL and bulk solution. In later derivations, E_z^* will be used as the normalizing velocity for velocity components. $\hat{D}_{0,1,2\ldots n}$ are given earlier in equation (7), and $\hat{G}_{0,1,2\ldots n}$ are Fourier series coefficients to be determined by applying the slip-stick boundary conditions:

$$w(R,\hat{z}) = \begin{cases} -\hat{\lambda}\partial w/\partial \hat{z} & 0 < \hat{z} < a\hat{l} \\ 0 & a\hat{l} < \hat{z} < \hat{l} \end{cases} \tag{13}$$

The mean velocity of the flow is given as:

$$\overline{w} = -\left[2\frac{\hat{D}_0}{\hat{\kappa}} \frac{I_1(\hat{\kappa})}{I_0(\hat{\kappa})} + \hat{G}_0 \right] E_z^* \tag{14}$$

2.3 Hydrodynamic dispersion

A homogenization analysis is performed to derive the dispersion coefficient due to the electro-osmotic flow. The idea of the homogenization technique (Mei 1992; Mei *et al*, 1996) is to deduce cell boundary-value problems at successive orders through introducing multiple-scale variables and expansions. In the present problem, two distinct length scales exist: the micro length scale represented by the channel radius or periodic length $R \sim l$ (denoted by the microscale coordinate r and z), and the macro length scale L beyond which the solute cloud distributes axially (denoted by the macroscale coordinate Z). The ratio of the two length scales is a small order parameter for the problem, i.e. $\varepsilon = l/L << 1$. Three time scales arise from the two length scales: a short time scale for diffusion over the micro length scale $t_0 = R^2/D \sim l^2/D$ (D is the molecular diffusivity), an intermediate time scale for advection over the macro length scale $t_1 = L/\overline{w}$ ($\overline{w}$ is the axial mean velocity), and a long time scale for diffusion over the macro length scale $t_2 = L^2/D$. Estimation of the three time scales relies on the magnitude of the Péclet number $\mathrm{Pe} = \overline{w}(2R)/\mathrm{D} = 2\,\mathrm{Re}\cdot(\nu/D)$, a dimensionless number denoting ratio of the convection rate and diffusion rate. For low-Reynolds number flows in microfluidic devices, many species of interest are large and slowly diffusing, and ν/D is usually high, but of finite value (e.g. $D = 10^{-9} m^2/s$ for salt in water at room temperature, whereas $\nu = 10^{-6} m^2/s$, herby $\nu/D = 10^3$). In this regard, we assume Pe to be on the order of unity $O(1)$ for generality. Estimation of the time scales can thus be obtained: $T_2 = T_1/\varepsilon = T_0/\varepsilon^2$. If $\mathrm{Pe} = O(\varepsilon^{-1})$ or $\mathrm{Pe} = O(\varepsilon)$ for special species, these estimates can be much different, and the subsequent asymptotic analysis needs to be modified accordingly.

Based on the aforementioned length and time scales, a multiple-scale asymptotic analysis can be performed on the transport equation:

$$\frac{\partial C}{\partial t} + \nabla\cdot(\vec{u}C) = D\nabla^2 C \tag{15}$$

where $C = C(r, z, Z, t)$ is the concentration, which is a time-dependent function of the fast spatial variables (r, z) and slow spatial variable (Z). $\vec{u} = (u, w)$ is the velocity vector.

Due to the periodic pattern on the microscale, the effective transport equation, which is purely with respect to the macroscale coordinate Z, can be obtained by means of spatial averaging over the microscale coordinates. Following the procedures presented by Mei *et al* (1996), the concentration, time derivative and spatial derivative are first expanded as power series of ε:

$$C \to C_0 + \varepsilon C_1 + \varepsilon^2 C_2 + \cdots, \tag{16}$$

$$\frac{\partial}{\partial t} \to \varepsilon \frac{\partial}{\partial t_1} + \varepsilon^2 \frac{\partial}{\partial t_2} + \cdots, \quad \frac{\partial}{\partial z} \to \frac{\partial}{\partial z} + \varepsilon \frac{\partial}{\partial Z} + \cdots \tag{17}$$

where C_0 denotes the leading-order concentration, and is independent of the microscale coordinates. At $O(\varepsilon)$, the first-order concentration is related to the leading-order concentration by:

$$C_1 = -N \frac{\partial C_0}{\partial Z}, \tag{18}$$

where $N(r, z)$ is a periodic function determined by the canonical boundary-value problem of Oseen type:

$$\begin{gathered} \nabla \cdot (\vec{u} N) - D \nabla^2 N = w - \bar{w}, \\ (0 < z < 2l, 0 < r < R) \end{gathered} \tag{19}$$

$$\begin{gathered} \frac{\partial N}{\partial r} = 0 \\ (r = R) \end{gathered} \tag{20}$$

The effective transport equation can be attained at the second order of perturbation $O(\varepsilon^2)$:

$$\frac{\partial C_0}{\partial t} + \bar{w} \frac{\partial C_0}{\partial Z} = (D + D_T) \frac{\partial^2 C_0}{\partial Z^2} \tag{21}$$

where D_T is the Taylor dispersion coefficient we aim to reach:

$$D_T = \left\langle \overline{Nw} - \bar{N}\bar{w} \right\rangle = \left\langle \overline{Nw} \right\rangle - \left\langle \bar{N} \right\rangle \bar{w} \tag{22}$$

the over bar and angle brackets above indicate cross-section averaging and axial averaging, respectively:

$$\bar{f} = \frac{2}{R^2} \int_0^R f r dr = 2 \int_0^1 f \hat{r} d\hat{r} \tag{23}$$

$$\langle f \rangle = \frac{1}{2l} \int_0^{2l} f dz = \frac{1}{2\hat{l}} \int_0^{2\hat{l}} f d\hat{z} \tag{24}$$

On introducing the following normalization:

$$\left(\hat{u}, \hat{w}, \hat{\bar{w}}\right) == (u, w, \bar{w}) / E_z^*, \quad \hat{N} = \left(\frac{D}{E_z^* R^2} \right) N, \quad \hat{D}_T = \left(\frac{D}{E_z^{*2} R^2} \right) D_T \tag{25}$$

equations (19) and (20) can be written in the dimensionless forms as below:

$$\mathrm{Pe}\left(\hat{w}\frac{\partial \hat{N}}{\partial \hat{z}}+\hat{u}\frac{\partial \hat{N}}{\partial \hat{r}}\right)-\frac{\partial^2 \hat{N}}{\partial \hat{z}^2}-\frac{1}{\hat{r}}\frac{\partial}{\partial \hat{r}}\left(\hat{r}\frac{\partial \hat{N}}{\partial \hat{r}}\right)=\hat{w}-\hat{\bar{w}}, \tag{26}$$
$$(0<\hat{z}<2\hat{l},0<\hat{r}<1)$$

$$\frac{\partial \hat{N}}{\partial \hat{r}}=0 \tag{27}$$
$$(r=1)$$

and the dimensionless Taylor dispersion coefficient $\hat{D}_T$, is readily to be found as:

$$\hat{D}_T=\left\langle\overline{\hat{N}\hat{w}}\right\rangle-\left\langle\hat{\bar{N}}\right\rangle\hat{\bar{w}} \tag{28}$$

Since the Oseen type equation (26) cannot be solved analytically, we next employ packages MATLAB and COMSOL to compute $\hat{D}_T$ numerically (figure 1(b)). Specifically, the dispersion coefficient is obtained through numerical simulation using the Convection and Diffusion model in COMSOL. The governing equation (26) and its boundary condition equation (27) are applied via settings in the physics module of the model. The velocity components for different sets of controlling parameters are first calculated using MATLAB, then output and exported into the model as constants and scalar expressions. Next, the model is initiated to solve the problem. After solution, the dispersion coefficient expressible by a global expression in the model via subdomain projection and boundary integration can be read from the result. Accuracy of the model built on COMSOL is verified through comparing results with theoretical limits obtained from lubrication approximation, known as the long-wave limits (see Appendix).

3. Numerical results

In the present problem, controlling parameters of the dispersion coefficient $\hat{D}_T$ include: (i) the normalized period length $\hat{l}$, (ii) the area fraction of the slipping region a (EOF-suppressing), (iii) the normalized zeta potential of the slipping region $\hat{\zeta}_S$, (iv) the normalized intrinsic slip length of the slipping region $\hat{\lambda}$, (v) the normalized Debye parameter $\hat{\kappa}$, and (vi) the Péclet number Pe. For the limiting case $\hat{l}\gg 1$ or $\hat{l}=\infty$, $\hat{D}_T$ becomes independent of $\hat{l}$ as well as Pe, and is computed from equation (32) in the Appendix as the long-wave limit. To address the question how the slipping region affects the overall hydrodynamic dispersion in EOF, we examine the dispersion coefficient $\hat{D}_T$ against the area fraction of the slipping region a, where it can be of different slip lengths and zeta potentials. An increasing a has two central effects that are decisive for behaviors of the dispersion, which we will clarify next.

First, the flow mean velocity behaves in different manners with the varying area fraction of the EOF-suppressing region a depending on the zeta potential and period length (see $\hat{\bar{w}}$ in figures 5 and 6), which causes the dispersion to change accordingly. In the two cases we are going to analyze, the original profile of

$\hat{\bar{w}}$ when slippage is absent presents a monotonically decreasing trend, plus, is independent of the period length. On introducing slippage, the trend is essentially still a monotonically decreasing one but no longer independent of $\hat{l}$ if the slipping region is uncharged (i.e. $\hat{\zeta}_S = 0$). Moreover, an abrupt drop near $a = 1$ is found for a relatively large $\hat{l}$ (e.g. $\hat{l} = 5$). When the slipping region is positively charged (e.g. $\hat{\zeta}_S = 0.5$), however, the trend is reversed into a monotonically increasing one dependent of $\hat{l}$. An abrupt change near $a = 1$ is also found, but an upsurge this time, and it is for a relatively small $\hat{l}$ (e.g. $\hat{l} = 1$). These behaviors of the mean velocity are consistent with the findings of Chu and Ng (2012).

Second, the effect imposed on the dispersion by the induced pressure-driven flow presents a non-monotonic trend against a (see the pressure-related components G^2 and $G\hat{\zeta}$ in figures 5 and 6), which is characterized by an up-down curve with a local extremum at an intermediate a. If the channel wall is non-slipping, the profiles of G^2 and $G\hat{\zeta}$ are exactly symmetric about $a = 0.5$, where the extremum appears. This symmetry can be easily understood through equations (37) and (38) in the Appendix obtained using the lubrication theory, both of which include the factor $a(1-a)$. Literally, $a = 0.5$ means that the channel has an equal fraction of EOF-suppressing and EOF-supporting regions. In other words, with only non-uniformity of zeta potential, the enhancing effect on the dispersion due to the induced pressure gradients is most significant when the channel wall is most heterogeneous (i.e. $a = 0.5$), but vanishes when the channel wall tends to be homogeneous (i.e. $a = 0$ or $a = 1$). The introduction of slippage further alters this non-monotonic effect in multiple fashions, which are illustrated in figures 5 and 6.

These two effects mentioned above, whose strength of influence on the dispersion is subject to controlling parameters $\hat{l}$, $\hat{\zeta}_S$, $\hat{\lambda}$, $\hat{\kappa}$, give rise to rich behaviors of $\hat{D}_T$ against a via interacting with each other in various configurations. To better evaluate the dispersion in different configurations for achieving efficient separation in microfluidic applications, appeal is also made to the plate height:

$$H_P = d\sigma^2(x_c)/dx_c \tag{29}$$

which describes the changes in the squared variance of the solute band due to mass transport for a unit distance. Herein, $\sigma(t)$ is the time-dependent band variance characterizing the solute band width, and $x_c(t)$ is the time-dependent coordinate of the mass center (figure 3). In the context of dispersion, the plate height indicates the spreading rate of the solute cloud per unit distance it moves and serves a useful measure of the band broadening. For an inert solute considered in the present problem, H_P is related to the dispersion coefficient D_T as given by (Zholkovskij *et al* 2010):

$$H_P = \frac{2D_T}{\bar{w}} \tag{30}$$

where $\bar{w} = dx_c/dt$ is the mean velocity of the mass center (equal to the mean velocity of the flow). The advantage of H_P over D_T in evaluating and comparing dispersion lies in that it provides a more intuitive

measure of the separation efficiency by addressing the mean velocity $\bar{w}$, while D_T simply indicates the dispersion strength. The mean velocity, known to impact the dispersion coefficient, also determines the mean residence time of the solute cloud, which can be interpreted as the convection time for an inert species spreading through a sufficiently long channel.

The Debye parameter $\hat{\kappa}$ is a pivotal factor for EOF, which directly decides thickness of the EDL forming near the charged wall (no EDL will form if the wall is uncharged). Given its importance, before proceeding to behaviors of the dispersion, we first elucidate the manner that $\hat{\kappa}$ influences the dispersion due to pure EOF, where no induced pressure-driven flow is considered. In the long-wave limit, the dispersion has exact analytical solutions to be presented with a straightforward diagram of interrelationship. For simplicity, we consider $\hat{\zeta}_S = 1$ so that the channel wall is uniformly charged. Under these conditions, the dispersion coefficient $\hat{D}_T$ reduces to X_e, given by equation (35). As demonstrated in figure 4, $X_e(\hat{\kappa})$ increases at first and reaches a maximum value of 0.00382775 at $\hat{\kappa} = 4.67968$, then it decreases and eventually becomes infinitesimally small as $\hat{\kappa} \to O(10^2)$. Physically, it means that for EOF with a very thin EDL, the hydrodynamic dispersion is negligible and the dispersion coefficient is vanishingly small.

3.1 Slipping region uncharged

When $\hat{\zeta}_s = 0$, the slipping regions are uncharged. Analytical proof was previously given by Squires (2008) and Chu and Ng (2012) that EOF experiences no enhancement from such regions, and if the surfaces are only partial-slipping, EOF will even be inhibited, whether in the thin EDL limit (practically achieved when $\hat{\kappa} > O(10^3)$) or not. The effect imposed by the uncharged slipping regions on the dispersion due to the EOF, however, can be either inhibitive or conducive depending on the Debye parameter $\hat{\kappa}$ (figures 7 and 8). When $\hat{\kappa}$ is small (e.g. $\hat{\kappa} = 10$), corresponding to a relatively thick EDL, the slipping region does inhibit the dispersion, namely, $\hat{D}_T$ decreases as the area fraction a increases. The physical reasoning can be given as below: for a small $\hat{\kappa}$, the EDL has a finite thickness, and the typical plug-like velocity profile of pure EOF fails to materialize, thus leading to considerate dispersion. $\hat{D}_T$ in this situation appears more susceptible to the EOF mean velocity $\hat{\bar{w}}$, which is monotonically decreasing against a here (figure 5). Alternatively speaking, the decreasing effect of $\hat{\bar{w}}$ outweighs the monotonic effect of the induced pressure-driven flow. When $\hat{\kappa}$ is moderately large (e.g. $\hat{\kappa} = 100$), the EDL is vanishingly thin and approximates to the thin EDL limit, the effect of the slipping region in this situation presents a non-monotonic trend, characterized by an up-down manner of $\hat{D}_T$ with a, and the inhibitive effect prevails only when the slip is large enough. This is because the contribution of pure EOF to the dispersion vanishes due to a virtually uniform velocity profile in this case, and the non-monotonic effect by the induced pressure-driven flow on the dispersion becomes dominant. For behaviors of the plate height, the non-monotonic trend manifests

itself more prominently. Even for a small Debye parameter $\hat{\kappa}=10$, an evident non-monotonic curve of $\hat{H}_P$ can already be gained provided that $\hat{\lambda}$ is relatively small (e.g. $\hat{\lambda}$=0.1) and $\hat{l}$ is moderately large (e.g. $\hat{l}=5$). A general relation can be revealed via comparison of $\hat{D}_T$ and $\hat{H}_P$: a configuration that has the maximum dispersion coefficient does not necessarily yield the largest plate height, or the widest solute band due to dispersion. This disagreement is caused by the flow mean velocity $\hat{\bar{w}}$, which is related to the convection time of the solute band.

The role that slip plays is by and large a negative contribution to the dispersion, though several exceptions exist (i.e. when $\hat{\kappa}=10$, as $\hat{\lambda}$=1 increases to $\hat{\lambda}$=100, $\hat{D}_T$ increases rather than decreases as expected in $\hat{l}=1,5,\infty$). Consequently, the inhibitive effect of the slipping region is mostly strengthened as the slip length increases, whereas the non-monotonic effect is, on the contrary, weakened (with a smaller peak value). To understand the exceptions mentioned above, we further examine $\hat{D}_T$ against a continuous range of $\hat{\lambda}$ ($0.001\le\hat{\lambda}\le1000$) for $\hat{\kappa}=10$ in the long-wave limit. For simplicity, the slipping and non-slipping regions are considered to be evenly distributed, i.e. $a=0.5$. The result of this examination is given in the inset of figure 7(a). Interestingly, we observe a down-up-steady curve of $\hat{D}_T$ against $\hat{\lambda}$: when a small amount of slippage (e.g. $\hat{\lambda}$=0.001) is introduced, $\hat{D}_T$ is inhibited and the extent of inhibition increases as $\hat{\lambda}$ increases until $\hat{\lambda}$ approaches 1, when the inhibitive effect of $\hat{\lambda}$ becomes less strong and $\hat{D}_T$ starts to increase instead; as $\hat{\lambda}$ continues to increase and grows large enough (e.g. $\hat{\lambda}>O(10^2)$), $\hat{D}_T$ is saturated and becomes independent of $\hat{\lambda}$. This examination well explains the exceptions mentioned above, which also happen to the behaviors of the plate height $\hat{H}_P$ when $\hat{\kappa}=10$.

Concerning the influence of the period length, one can see that increasing $\hat{l}$ considerably amplifies the dispersion, especially when $\hat{\kappa}$ is relatively large (e.g. $\hat{\kappa}=100$). Meanwhile, for both $\hat{\kappa}=10$ and $\hat{\kappa}=100$, the non-monotonic effect due to the induced pressure-driven flow gains a larger influence as $\hat{l}$ increases, either altering a monotonically decreasing profile of $\hat{D}_T$ into a non-monotonic manner or prompting an original non-monotonic profile into a shaper curve. Despite an increased $\hat{l}$, however, the maximum of $\hat{D}_T$ appears at nearly the same a if other conditions are identical. In addition, $\hat{D}_T$ ends in zero at $a=1$, which corresponds to zero EOF simply because the channel wall is completely uncharged and no EDL exists. We pay particular attention to $\hat{H}_P$ in the limiting case $\hat{l}=\infty$, where it behaves in a distinctive manner from $\hat{D}_T$. To be specific, we state the difference in two aspects. First, $\hat{H}_P$ does not end in zero at $a=1$, but rather varies as different finite values depending on $\hat{\lambda}$. Second, the manner $\hat{H}_P$ changes with a is abnormal. When slippage is absent (i.e. $\hat{\lambda}$=0), $\hat{H}_P$ increases linearly and monotonically

as a increases, with a theoretical maximum plate height found at $a=1$ (though it actually corresponds to zero flow). On introducing slippage, this linearity becomes atypical, and $\hat{H}_P$ grows to be more non-monotonic as $\hat{\lambda}$ increases, except for $\hat{\kappa}=10$, $\hat{\lambda}$=100, when $\hat{H}_P$ decreases linearly and monotonically.

3.2 Slipping region charged

When $\hat{\zeta}_S=0.5$, the slipping regions are positively charged. Similar to last case where the slipping regions are uncharged, the effect imposed by these charged slipping regions on the dispersion also depends much on the Debye parameter $\hat{\kappa}$, small or large. Perceptually, a palpable alteration happens to the behavior of $\hat{D}_T$ in the current case: the non-monotonic effect gains a more predominant influence (compare figures 7 and 9). Even at a small $\hat{\kappa}$ (e.g. $\hat{\kappa}=10$), an evident non-monotonic curve can already be observed provided that the slip is appreciable (e.g. $\hat{\lambda}$=1,100). This enhanced non-monotonic effect can be attributed to two reasons. First, the EOF mean velocity $\hat{\bar{w}}$ in this case presents a monotonically increasing trend against a (figure 6), in contrast to the monotonically decreasing trend presented by the uncharged slipping region. Second, the monotonic effect by the induced pressure-driven flow itself grows stronger as the slipping region becomes charged, which is self-evident by comparing magnitudes of the pressure-related components G^2, $G\hat{\zeta}$ in the two cases (see figures 7 and 9). The trend of $\hat{H}_P$ against a basically resembles that of $\hat{D}_T$, and we leave it to be discussed later.

The role that slip plays in this case, opposing to that when the slipping regions are uncharged, mostly manifest itself as a positive contribution to the dispersion. The inhibitive effect of the slipping regions, if any, will thus be weakened by an increasing slip, while the non-monotonic effect will be strengthened (with a larger peak value). Still, several exceptions can be found for the inhibitive effect (i.e. when $\hat{\kappa}=10$, as $\hat{\lambda}$=0 increases to $\hat{\lambda}$=0.1, $\hat{D}_T$ decreases rather than increases as expected in $\hat{l}=5,\infty$). Again, to explain these exceptions, we further examine $\hat{D}_T$ against a continuous range of $\hat{\lambda}$ ($0.001\le\hat{\lambda}\le1000$) for $\hat{\kappa}=10$ in the long-wave limit assuming that the slipping regions and non-slipping regions are evenly distributed, i.e. $a=0.5$. The result of this examination is given in the inset of figure 9(c). Surprisingly, we find that when a small amount of slippage is initially introduced, e.g. $\hat{\lambda}$=0.001, $\hat{D}_T$ is actually reduced, not increased as expected. Furthermore, the degree of reduction increases as $\hat{\lambda}$ increases, until $\hat{\lambda}$ approaches $\hat{\lambda}=0.1$, when the negative effect of $\hat{\lambda}$ on $\hat{D}_T$ is weakened and $\hat{D}_T$ starts to increase ($\hat{D}_T$ is still smaller than the value when slippage is absent, i.e. $\hat{\lambda}$=0). As $\hat{\lambda}$ continues to increase, the negative effect reverses and turns to be positive effect on the dispersion. Eventually, $\hat{D}_T$ is saturated and becomes independent of $\hat{\lambda}$ when $\hat{\lambda}>O(10^2)$. Hereby, the exceptions mentioned above for $\hat{D}_T$ are well-explained, so are those for

$\hat{H}_P$ when $\hat{\kappa}=10$. It is noteworthy that for $\hat{\kappa}=10$, when the period length is short (e.g. $\hat{l}=1$), the slip exerts a negative contribution on the plate height $\hat{H}_P$ (increasing $\hat{\lambda}$ causes $\hat{H}_P$ to decrease), despite its positive effect on the dispersion coefficient $\hat{D}_T$.

Concerning the amplifying effect of the increasing period length $\hat{l}$ on the dispersion, we observe a manifest amplification, which can be several orders with the presence of an appreciable slip. For the non-monotonic effect due to the induced pressure-driven flow, it also gains a larger influence as $\hat{l}$ increases. In the limiting case $\hat{l}=\infty$, an abrupt drop of $\hat{D}_T$ occurs near $a=1$, which literally means that a slight deviation of a from this position can significantly decrease the dispersion. Different from the last case when the slipping regions are uncharged, an increased $\hat{l}$ in the current case will notably alter the critical value of a where the maximum of $\hat{D}_T$ occurs in the current case. Specifically at $a=1$, $\hat{D}_T$ is no longer zero, but of a finite value. This value is independent of $\hat{l}$ as well as $\hat{\lambda}$, and remains unchanged as long as $\hat{\kappa}$ is the same. Note that the value for $\hat{\kappa}=100$ is much smaller than that for $\hat{\kappa}=10$, for which the physical reasoning can be lent from our earlier elucidation of the influence of $\hat{\kappa}$ on the dispersion due to pure EOF. For $\hat{H}_P$, the finite value at $a=1$ is dependent of both $\hat{\kappa}$ and $\hat{\lambda}$. In particular for $\hat{\kappa}=10$, discrepancies of this value caused by an increasing $\hat{\lambda}$ are appreciable. When $\hat{\kappa}$ or $\hat{\lambda}$ is large enough, $\hat{H}_P$ vanishes and this finite value is essentially negligible.

4. Discussion

The asymptotic solution of the effective dispersion coefficient (long-time limit) of an inert solute in a homogeneous channel was given by the Taylor-Aris dispersion coefficient D_{eff} (Taylor 1953, Aris 1956):

$$D_{eff}=D+\gamma\frac{U^2L_C^2}{D}=D\left(1+\gamma\mathrm{Pe}^2\right) \tag{31}$$

which is the sum of the molecular diffusion and the Taylor dispersion. Herein, γ represents dispersivity, which equals to the well-known factor of 1/48 for pressure-driven flow in a homogeneous circular capillary. Pe represents the Péclet number defined as $\mathrm{Pe}=UL_C/D$, where U stands for the flow mean velocity, L_C the characteristic length, and D the molecular diffusivity. Physically, Pe indicates the importance of convection relative to diffusion in the transport process. One should bear in mind that the Taylor dispersion term arises from the non-uniformity of flow velocity, and vanishes for a uniform velocity. From equation (31), insight into how and flow mean velocity $\bar{w}$ and the Péclet number Pe in the present problem exert influence on $\hat{D}_T$ (corresponding to the Taylor dispersion item) can be gained.

Two phenomena that have opposing effects on hydrodynamic dispersion brought about by the non-uniformity of wall potential and hydrodynamic slip are essential and should be addressed. First, the flow

becomes two-dimensional in the vicinity of a step change in zeta potential or slip length. Because of the sudden change in boundary condition, transverse flow is induced near the discontinuity, thus enhancing mixing in the cross section. Transverse mixing is known to reduce dispersion in the axial direction. Though this mixing due is relatively local (confined to a small region with a dimension comparable to the channel radius near the discontinuity), its assembling effect on the system-average dispersion is not necessarily negligible. Second, pressure gradients are induced so as to maintain continuity of the flow through distinct regions of the channel because of the surface heterogeneities. The flow is a superposition of the original EOF and the induced pressure-driven flow. EOF has a nearly flat velocity profile for sufficiently large $\hat{\kappa}$, while pressure-driven flow presents a parabolic one. Consequently, the otherwise small dispersion in pure EOF can be substantially amplified by the induced pressure-driven flow. Different from the local decreasing effect on dispersion due to transverse flow, this increasing effect of pressure-driven flow is global, since the induced pressure gradients, once induced, will be effective throughout the whole channel. These two opposing effects will have different degrees of influence on the dispersion coefficient depending on controlling parameters $\hat{l}$, a, $\hat{\zeta}_s$, $\hat{\lambda}$, $\hat{\kappa}$ and Pe, leading to rich behaviors of $\hat{D}_T$.

4.1 Numerical accuracy

To verify the accuracy of the numerical model built on COMSOL, we compare numerical results with corresponding long-wave limits and check whether they approximate to the latter for a period length that is large enough. To this end, we examine the dispersion coefficient $\hat{D}_T$ against the period length $\hat{l}$ for a Debye parameter of $\hat{\kappa}=10$ subject to $\hat{\zeta}_S$, a and Pe. As a preliminary examination, the channel wall is considered to be non-slipping and only step change of zeta potential is present. The model is proved to yield reasonable results, and multiple dependence of $\hat{D}_T$ on $\hat{l}$, $\hat{\zeta}_S$, a and Pe are found (figure 11). Some rules Ng and Chen (2013) revealed earlier for electro-osmotic dispersion in a non-slipping slit channel with axial step change of zeta potential are applicable here as well:

(I) $\hat{D}_T$ increases as the period length $\hat{l}$ gets larger, gradually approaching the long-wave limit. This is the compromised result of the two opposing effects mentioned earlier. For a small $\hat{l}$, discontinuities in the wall pattern are closely spaced, and the overall suppressing effect on the dispersion by transverse flows near these discontinuities is dominant. For a large $\hat{l}$, the discontinuities are distributed sparsely, and the enhancing effect on the dispersion by the induced pressure-driven flow outweighs the suppressing effect by the transverse flows. The gap between the numerical result and the long-wave limit gradually narrows down as $\hat{l}$ increases. Nevertheless, the discrepancy is still notable even when the period length increases to 10~20, especially for a small Debye parameter (figure 11(a)).

(II) $\hat{D}_T$ is more sensitive to the period length $\hat{l}$ when the contrast of zeta potentials in the EOF-suppressing region and the EOF-supporting region is larger, which is indicated by the value of $\hat{\zeta}_S$. A larger

contrast of the zeta potentials has two-sided effects. On one hand, a stronger transverse flow will be generated near the discontinuity of the step change; on the other, the pressure-driven flow also grows stronger due to larger pressure gradients induced to maintain flow continuity. To put it differently, both of the two opposing effects are strengthened. Therefore, the interaction between them is intensified, resulting in a more drastic change of $\hat{D}_T$ as $\hat{l}$ varies.

(III) $\hat{D}_T$ is more sensitive to the period length $\hat{l}$ when the slipping area fraction a has an either small or large value. For a short or moderate period length, the absolute difference between the numerical result and the long-wave limit is small when $a = 0.1$ or $a = 0.9$, but can be very large when a has an intermediate value (e.g. $a = 0.3, 0.5, 0.7$). This implies that, the more homogeneous the channel wall is, the better the long-wave limit estimates the actual dispersion coefficient.

(IV) $\hat{D}_T$ decreases as the Péclet number Pe increases. When Pe increases, the convection gradually outweighs molecular diffusion in controlling mass transport over the micro length scale, thus contributing to cross-sectional mixing due to the transverse flow near the discontinuity. This enhanced transverse mixing effect amounts to further decreased dispersion, which is manifest for a short or moderate period length.

4.2 Validity of the lubrication approximation

We next investigate the validity of the lubrication approximation approach in estimating electro-osmotic dispersion in the slip-stick patterned channel by adding $\hat{\lambda}$ as a controlling parameter. For a specific configuration shown in figure 12 (note that we have deliberately chosen a configuration where the long-wave limit relatively gives a better estimation for the situation with no-slip), with the presence of slippage, the dispersion coefficient can be substantially overestimated if the long-wave limit is adopted even for a period 10~20 times as long as the channel radius. Furthermore, the error of estimation is enlarged if a larger slip is introduced. Table 1 gives exact numbers of the error. When slippage is absent, the error caused is only 1.4% for a relatively large period length $\hat{l} = 20$, and the lubrication approximation can be reasonably justified. However, with an appreciable slip $\hat{\lambda} = 1$, the error drastically increases to 17.4%, and 22.5% for $\hat{\lambda} = 100$ (used to approximate perfect-slip here). It is clear that the lubrication approximation can no longer be justified with such large errors.

5. Concluding remarks

We have reaffirmed some earlier remarks on the accuracy of the lubrication approximation approach in estimating the dispersion due to electro-osmotic flow in a non-slipping channel with step-wise pattered zeta potential. When the period length of the wall pattern is short or only moderately large, the transverse mixing near the discontinuities ignored by the lubrication approximation is significant, especially for a configuration with a large zeta potential contrast but a small fraction difference of the two distinct regions

and a high Péclet number. Under these conditions, the dispersion can be substantially overestimated if the long-wave limit is used. The error will be further enlarged if slip is present on the wall.

It is remarkable that the introduction of wall slip brings about more intensive behaviors of the hydrodynamic dispersion than the situation with no-slip boundary condition, as the slip interacts with zeta potentials in the EOF-suppressing and EOF-supporting regions. To be brief, slip in an unchanged EOF-suppressing region is shown to suppress the effect of the induced pressure-driven flow on the dispersion, and diminish the dispersion on the whole. In contrast, slip in a charged EOF-suppressing region will mostly enhance the effect of the induced pressure-driven flow, and amplify the overall dispersion.

The non-uniformities of the wall potential and hydrodynamic slip yield multiple dispersion coefficients and plate heights subject to various controlling parameters. One can tailor the flow for particular microfluidic applications by adjusting these controlling parameters. If separation is wanted, the configuration with a smaller plate height as well as dispersion coefficient should be adopted (the plate height is a priority if conflicts exist); if mixing is wanted, the opposite is desired.

Acknowledgments

The authors gratefully acknowledge comments by the two reviewers. This work was financially supported by the Research Grants Council of the Hong Kong Special Administrative Region, China, through projects HKU 715609E and HKU 715510E.

Appendix: long-wave limit ($\hat{l} \gg 1$)

In a study on dispersion due to EOF in a circular microchannel with slowly varying wall potential and hydrodynamic slippage, the long-wave limit of the dispersion is given by Ng and Zhou (2012b):

$$\hat{D}_T(\hat{z}) = X_p \left\langle G^2(\hat{z}) \right\rangle + X_{pe} \left\langle G(\hat{z})\hat{\zeta}(\hat{z}) \right\rangle + X_e \left\langle \hat{\zeta}^2(\hat{z}) \right\rangle \tag{32}$$

wherein,

$$X_p = \frac{1}{48}, \tag{33}$$

$$X_{pe}(\hat{\kappa}) = \left(\frac{1}{6\hat{\kappa}} - \frac{4}{\hat{\kappa}^3} - \frac{32}{\hat{\kappa}^5} \right) \frac{I_1(\hat{\kappa})}{I_0(\hat{\kappa})} + \frac{16}{\hat{\kappa}^4}, \tag{34}$$

$$X_e(\hat{\kappa}) = \left(\frac{3}{2\hat{\kappa}^2} + \frac{8}{\hat{\kappa}^4} \right) \frac{I_1^2(\hat{\kappa})}{I_0^2(\hat{\kappa})} - \frac{2}{\hat{\kappa}^3} \frac{I_1(\hat{\kappa})}{I_0(\hat{\kappa})} - \frac{1}{\hat{\kappa}^2} \tag{35}$$

In equation (32), G^2 and $\hat{\zeta}^2$ are components associated with the pressure-driven flow caused by the induced pressure gradients and the electrically driven flow intrigued by the externally applied electric field, respectively. The other component $G\hat{\zeta}$ can be interpreted as a term due to the interaction between these two flows; in this regard, it is associated with both flows. X_p, X_e and X_{pe} are the corresponding pre-

factors, which are all independent of the slip and physically serve as magnitude estimates of the contributions from the three components to the total dispersion. The expression of $\hat{D}_T$ given by equation (32) can be used to calculate the long-wave limits in different configurations as references for the numerical results. When examining the effect imposed by the induced pressure-driven flow on the dispersion coefficient, the behaviors of G^2 and $G\hat{\zeta}$ can be reasonable indicators to look at. Though relations developed in the constraint of long-wave limit may not be identical with those for the dispersion in a general case where the period length is comparable to the channel dimension, they suffice to reflect the inclination, if not quantitatively, qualitatively.

In the particular case where no slippage exists on the wall and the periodic pattern involves only step change in the zeta potential:

$$\hat{\zeta}(\hat{z}) = \begin{cases} \hat{\zeta}_s & 0 < \hat{z} < a \\ 1 & a < \hat{z} < 1 \end{cases}, \qquad \hat{\delta}(\hat{z}) = \begin{cases} 0 & 0 < \hat{z} < a \\ 0 & a < \hat{z} < 1 \end{cases} \tag{36}$$

The following can be readily found:

$$\left\langle \hat{\zeta}^2(\hat{z}) \right\rangle = -a(1-\hat{\zeta}_S{}^2) + 1, \tag{37}$$

$$\left\langle G^2(\hat{z}) \right\rangle = a(1-a)\left[1 - \frac{2}{\hat{\kappa}}\frac{I_1(\hat{\kappa})}{I_0(\hat{\kappa})}\right]^2 (1-\hat{\zeta}_S)^2 , \tag{38}$$

$$\left\langle G(\hat{z})\hat{\zeta}(\hat{z}) \right\rangle = -a(1-a)\left[1 - \frac{2}{\hat{\kappa}}\frac{I_1(\hat{\kappa})}{I_0(\hat{\kappa})}\right](1-\hat{\zeta}_S)^2 \tag{39}$$

From above, we can get a glimpse of how the area fraction of the EOF-suppressing region will affect the dispersion coefficient through electric and pressure components, especially the latter, which apparently present a non-monotonic effect with the maxima/minima appearing at $a = 0.5$. On introducing slippage, this non-monotonic effect can be altered in various ways, as seen in figures 5 and 6.

References

Ajdari A 1996 Generation of transverse fluid currents and forces by an electric field: Electro-osmosis on charge-modulated and undulated surfaces *Phys. Rev. Lett.* 53 4996-5005

Anderson J L and Idol W K 1985 Electroosmosis through pores with nonuniformly charged walls *Chem. Eng. Commum.* 38 93-106

Aris R 1956 On the dispersion of a solute in a fluid flowing through a tube *Proc. R. Soc. Lond., Ser. A* 235 67-77

Bahga S S, Vinogradova O I and Bazant M Z 2010 Anisotropic electro-osmotic flow over super-hydrophobic surfaces *J. Fluid Mech.* 644 245

Belyaev A V and Vinogradova O I 2011 Electro-osmosis on anisotropic superhydrophobic surfaces *Phys. Rev. Lett.* 107 098301

Celia E, Darmanin T, Taffin de Givenchy E, Amigoni S and Guittard F 2013 Recent advances in designing superhydrophobic surfaces *J. Colloid Interface Sci.* 402 1-18

Chu H C W and Ng C O 2012 Electroosmotic flow through a circular tube with stick-slip striped wall *J. Fluid. Eng.* 134 111201

Datta S and Choudhary J N 2013 Effect of hydrodynamic slippage on electro-osmotic flow in zeta potential patterned nanochannels *Fluid Dyn. Res.* 45 055502

Datta S and Ghosal S 2009 Characterizing dispersion in microfluidic channels *Lab Chip* 9 2537-50

Datta R and Kotamarthi V R 1990 Electrokinetic dispersion in capillary electrophoresis. *AIChE J.* 36 916

Dawson K and O'Riordan A 2014 Electroanalysis at the nanoscale *Annu. Rev. Anal. Chem.* 7 163-81

Devasenathipathy S and Santiago J G Electrokinetic flow diagnostics *Microscale Diagnostic Techniques* (Springer-Verlag, Berlin Heidelberg, Germany, 2005) 113-154

Ghosal S 2002a Lubrication theory for electro-osmotic flow in a microfluidic channel of slowly varying cross-section and wall charge *J. Fluid Mech.* 459 103-128

Ghosal S 2002b Band broadening in a microcapillary with a stepwise change in the ζ-potential *Anal. Chem.* 74 4198-203

Ghosal S 2003 The effect of wall interactions in capillary-zone electrophoresis *J. Fluid Mech.* 491 285-300

Ghosal S 2006 Electrokinetic flow and dispersion in capillary electrophoresis *Annu. Rev. Fluid Mech.* 38 309-38

Griffiths S K and Nilson R H 1999 Hydrodynamic dispersion of a neutral nonreacting solute in electroosmotic flow *Anal. Chem.* 71 5522-9

Griffiths S K and Nilson R H 2000 Electroosmotic fluid motion and late-time solute transport for large zeta potentials *Anal. Chem.* 72 4767-77

Herr A E, Molho J I, Santiago J G, Mungal M G and Kenny T W 2000 Electroosmotic capillary flow with nonuniform zeta potential *Anal. Chem.* 72 1053-7

Huang D M, Cottin-Bizonne C, Ybert C and Bocquet L 2008 Massive amplification of surface-induced transport at superhydrophobic surfaces *Phys. Rev. Lett.* 101 064503

Long D, Stone H A and Ajdari A 1999 Electroosmotic flows created by surface defects in capillary electrophoresis *J. Colloid Interface Sci.* 212 338-49

Martin M and Guiochon G 1984 Axial dispersion in open-tubular capillary liquid chromatography with electroosmotic flow *Anal. Chem.* 56 614-20

Mei C C 1992 Method of homogenization applied to dispersion in porous media *Transp. Porous Med.* 9 261-348

Mei C C, Auriault J L and Ng C O 1996 Some applications of the homogenization theory *Adv. Appl. Mech.* 32 277-348

Muller V M, Sergeeva I P, Sobolev V D and Churaev N V 1986 Boundary effects in the theory of electrokinetic phenomena *Colloid J. USSR* 48 606

Ng C O and Chen B 2013 Dispersion in electro-osmotic flow through a slit channel with axial step change of zeta potential *J. Fluid. Eng.* 135 101203

Ng C O and Chu H C W 2011 Electrokinetic flows through a parallel-plate channel with slipping stripes on walls *Phys. Fluids* 23 102002

Ng C O and Zhou Q 2012a Electro-osmotic flow through a thin channel with gradually varying wall potential and hydrodynamic slippage *Fluid Dyn. Res.* 44 055507

Ng C O and Zhou Q 2012b Dispersion due to electroosmotic flow in a circular microchannel with slowly varying wall potential and hydrodynamic slippage *Phys. Fluids* 24 112002

Paul S and Ng C O 2012a Dispersion in electroosmotic flow generated by oscillatory electric field interacting with oscillatory wall potentials *Microfluid. Nanofluid.* 12 237-56

Paul S and Ng C O 2012b On the time development of dispersion in electroosmotic flow through a rectangular channel *Acta Mechanica Sinica* 28 631-43

Potoček B, Gaš B, Kenndler E and Štědrý M 1995 Electroosmosis in capillary zone electrophoresis with non-uniform zeta potential *J. Chromatogr. A* 709 51

Rothstein J P 2010 Slip on superhydrophobic surfaces *Annu. Rev. Fluid Mech.* 42 89-109

Schönecke C and Hardt S 2014 Electro-osmotic flow along superhydrophobic surfaces with embedded electrodes *Phys. Rev. E* 89 063005

Squires T M 2008 Electrokinetic flows over inhomogeneously slipping surfaces *Phys. Fluids* 20 092105

Steffes C, Baier T and Hardt S 2011 Enabling the enhancement of electroosmotic flow over superhydrophobic surfaces by induced charges *Colloids Surf., A* 376 85-8

Stroock A D and Whitesides GM 2003 Controlling flows in microchannels with patterned surface charge and topography *Acc. Chem. Res.* 36 597-604

Taylor G I 1953 Dispersion of soluble matter in solvent flowing slowly through a tube *Proc. R. Soc. Lond., Ser. A* 219 186-203

Zhao C and Yang C 2012 Electro-osmotic flows in a microchannel with patterned hydrodynamic slip walls *Electrophoresis* 33 899-905

Zhao H 2010 Electro-osmotic flow over a charged superhydrophobic surface *Phys. Rev. E* 81 066314

Zhao H 2011 Streaming potential generated by a pressure-driven flow over superhydrophobic stripes *Phys. Fluids* 23 022003

Zhao H and Bau H H 2007 Effect of secondary flows on Taylor-Aris dispersion *Anal. Chem.* 79 7792-8

Zholkovskij E K and Masliyah J H 2004 Hydrodynamic dispersion due to combined pressure-driven and electroosmotic flow through microchannels with a thin double layer *Anal. Chem.* 76 2708-18

Zholkovskij E K, Masliyah J H and Czarnecki J 2003 Electroosmotic dispersion in microchannels with a thin double layer *Anal. Chem.* 75 901-9

Zholkovskij E K, Yaroshchuk A E, Masliyah J H and Ribas J P 2010 Broadening of neutral solute band in electroosmotic flow through submicron channel with longitudinal non-uniformity of zeta potential *Colloids Surf., A* 354 338-46

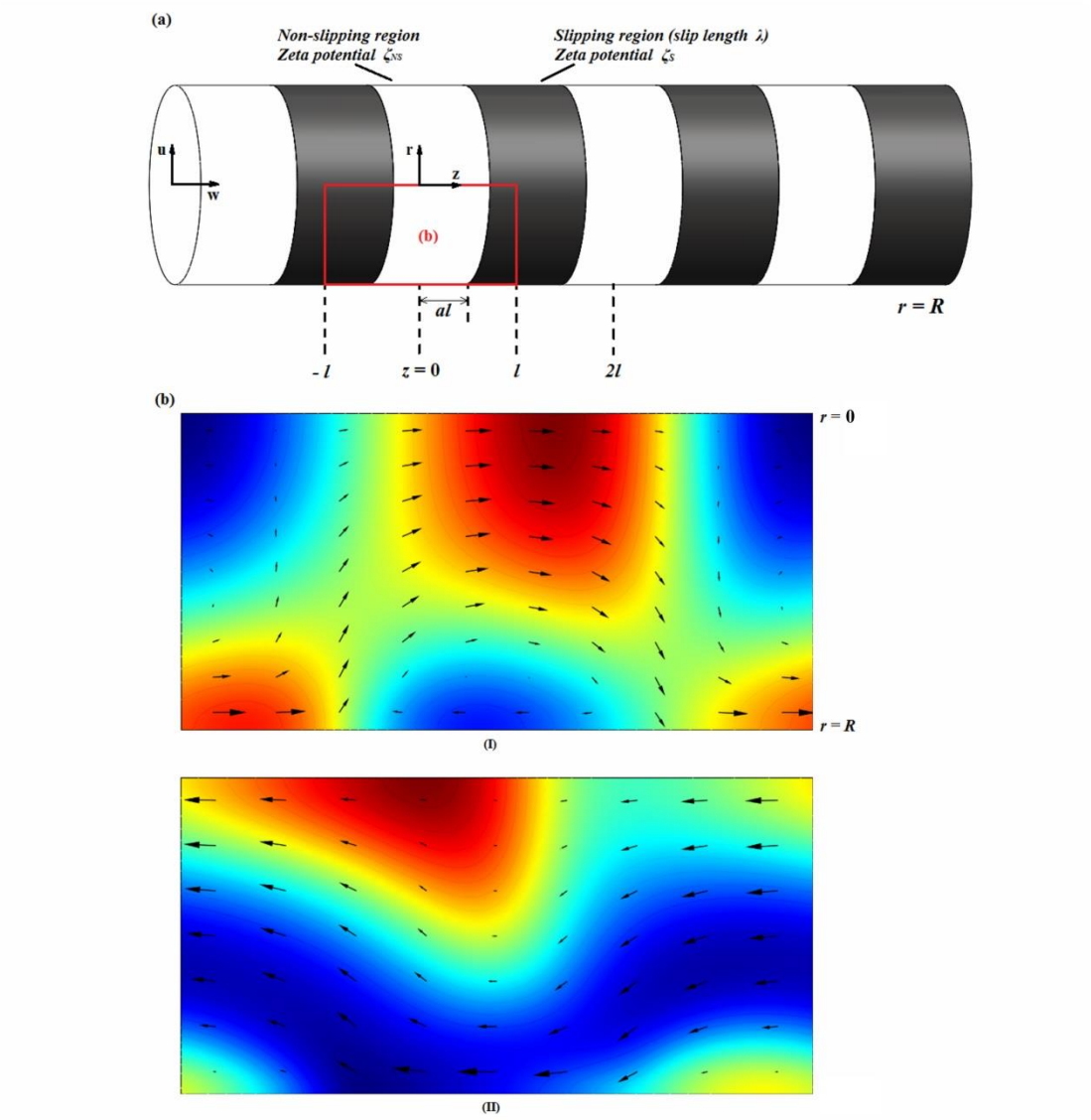

Figure 1. (a) Schematic of the electro-osmotic flow (EOF) through a circular tube with channel wall patterned with a periodic array of transverse stripes. The flow is two-dimensional in the (r, z) plane. The radial and axial coordinates are (r, z), and their corresponding velocity components are denoted by (u, w). One unit of wall pattern is 2*l*, consisting of a non-slipping stripe of zeta potential ζ_{NS}, and a slipping stripe of slip length λ and zeta potential ζ_S. The area fraction of the slipping region is denoted by a. (b) Mass concentration (see online color version. herein, a lower color temperature (e.g. red) indicates a higher mass concentration, and vice versa) of the EOF within the tube where $\hat{\zeta}_S = -0.5$, the slipping area fraction $a = 0.5$, period length $\hat{l} = 1$ ($\hat{l} = l / R$), Debye parameter $\hat{\kappa} = 100$ ($\hat{\kappa} = \kappa R$), and Péclet number $\mathrm{Pe} = 10$. (I) $\hat{\lambda} = 0.001$; (II) $\hat{\lambda} = 100$. Arrows indicate the local flow direction and velocity magnitude. In this configuration, flow reversal can happen due to the increase of $\hat{\lambda}$ as (II) shows.

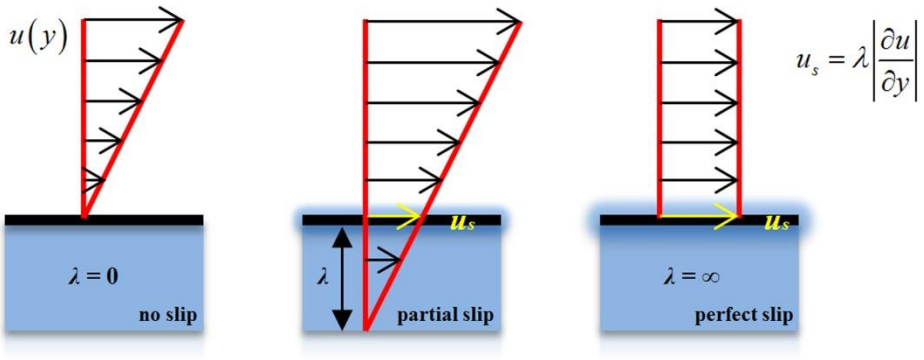

Figure 2. Navier's slip length

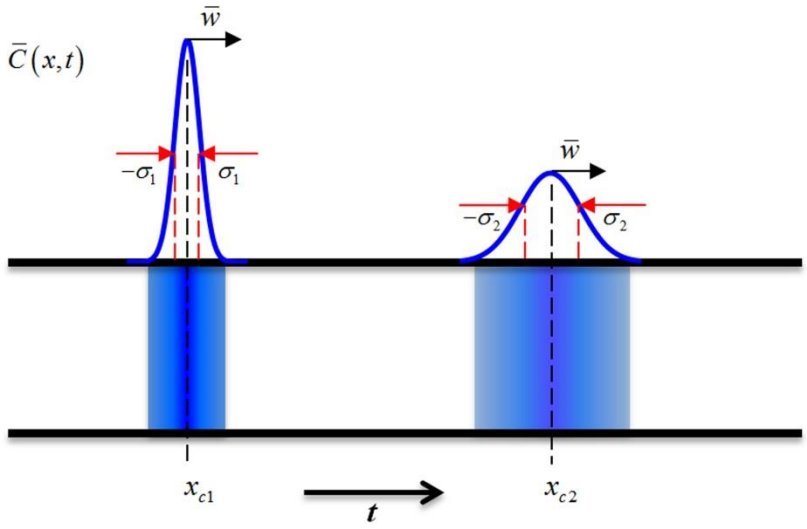

Figure 3. Schematic of solute band broadening ($t \geq L^2 / D$)

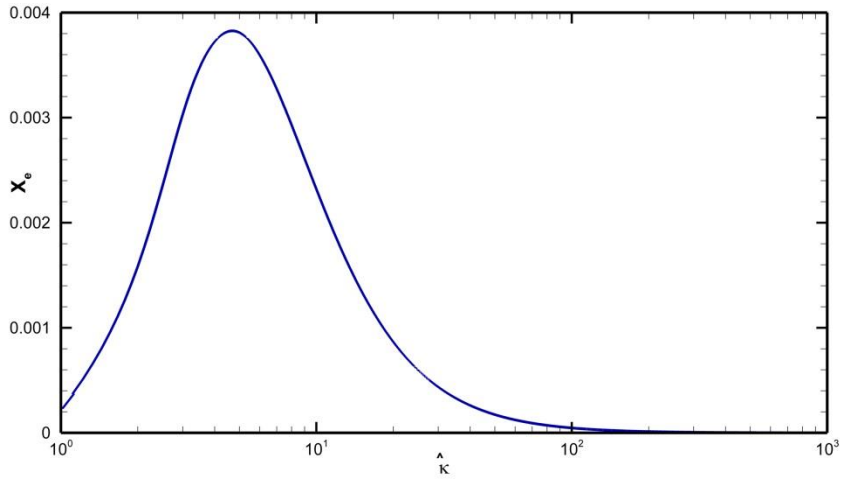

Figure 4. Dispersion coefficient $\hat{D}_T$ ($=X_e$ in this case) as a function of the Debye Parameter $\hat{\kappa}$ for pure EOF in a uniformly charged non-slipping channel ($\hat{\zeta}_S = 1$, $\hat{\lambda}=0$).

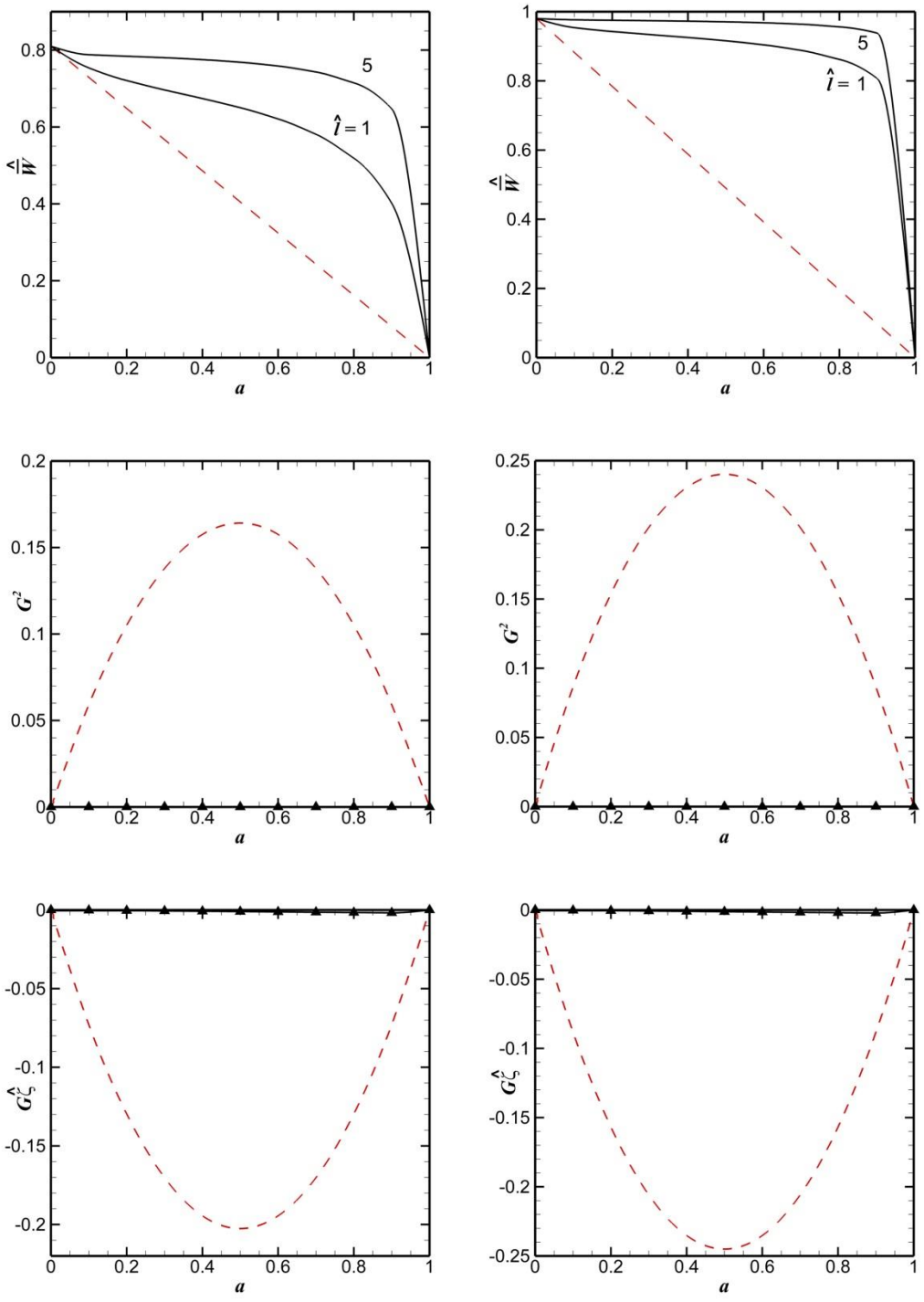

Figure 5. $\hat{\bar{w}}$, G^2 and $G\hat{\zeta}$ as functions of the slipping area fraction $0 \le a \le 1$, for $\hat{\kappa}=10,\ 100$ (from left to right), $\hat{\zeta}_S=0$, $\hat{\lambda}=0,\ 100$, $\mathrm{Pe}=10$, and $\hat{l}=1,\ 5$. The solid lines are for $\hat{\lambda}=100$, while the dashed lines are for $\hat{\lambda}=0$.

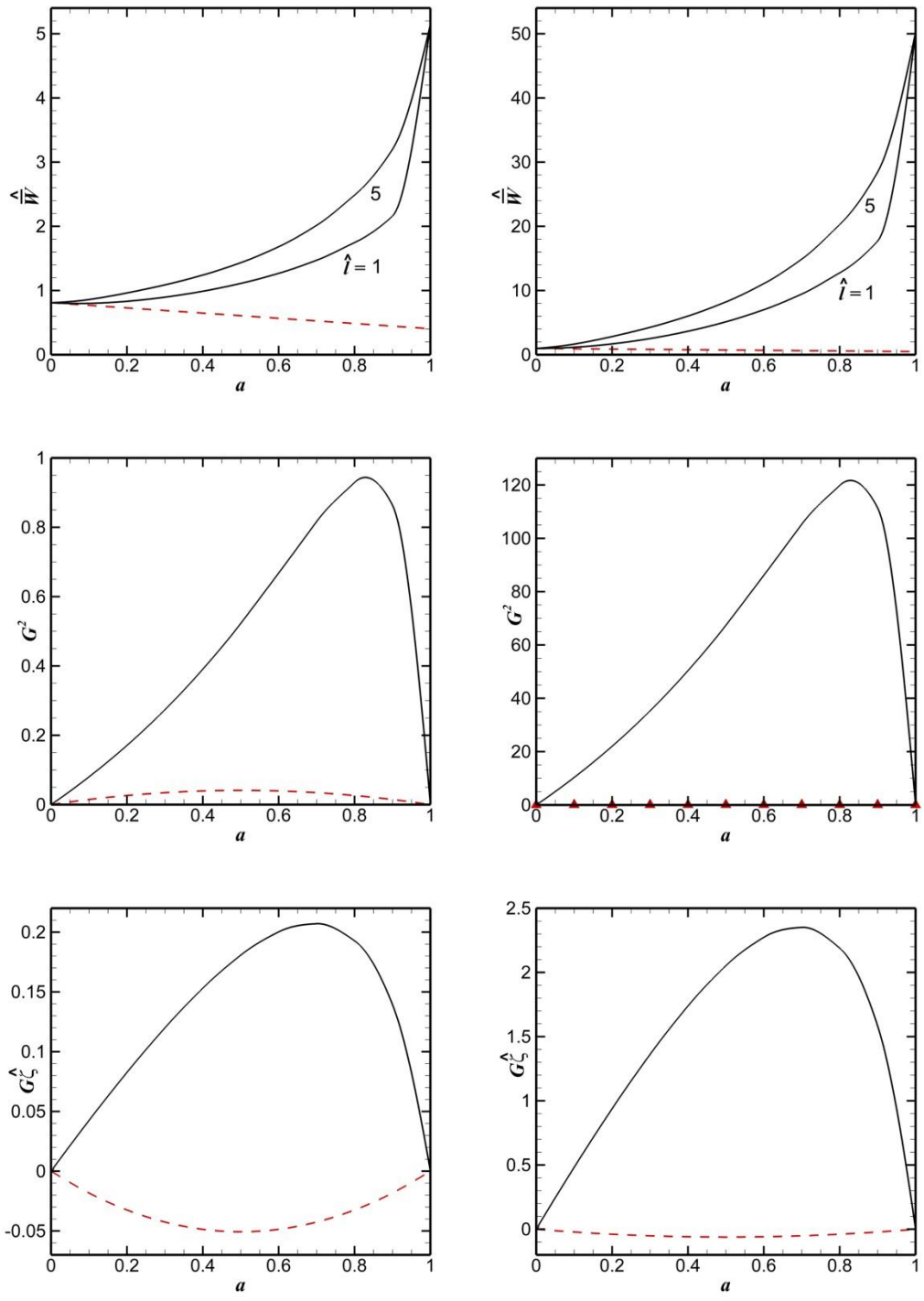

Figure 6. $\hat{\bar{w}}$, G^2 and $G\hat{\zeta}$ as functions of the slipping area fraction $0 \le a \le 1$, for $\hat{\kappa}=10,\ 100$ (from left to right), $\hat{\zeta}_S = 0.5$, $\hat{\lambda}=0,\ 1,$ $\mathrm{Pe}=10$, and $\hat{l}=1,\ 5$. The solid lines are for $\hat{\lambda}=1$, while the dashed lines are for $\hat{\lambda}=0$.

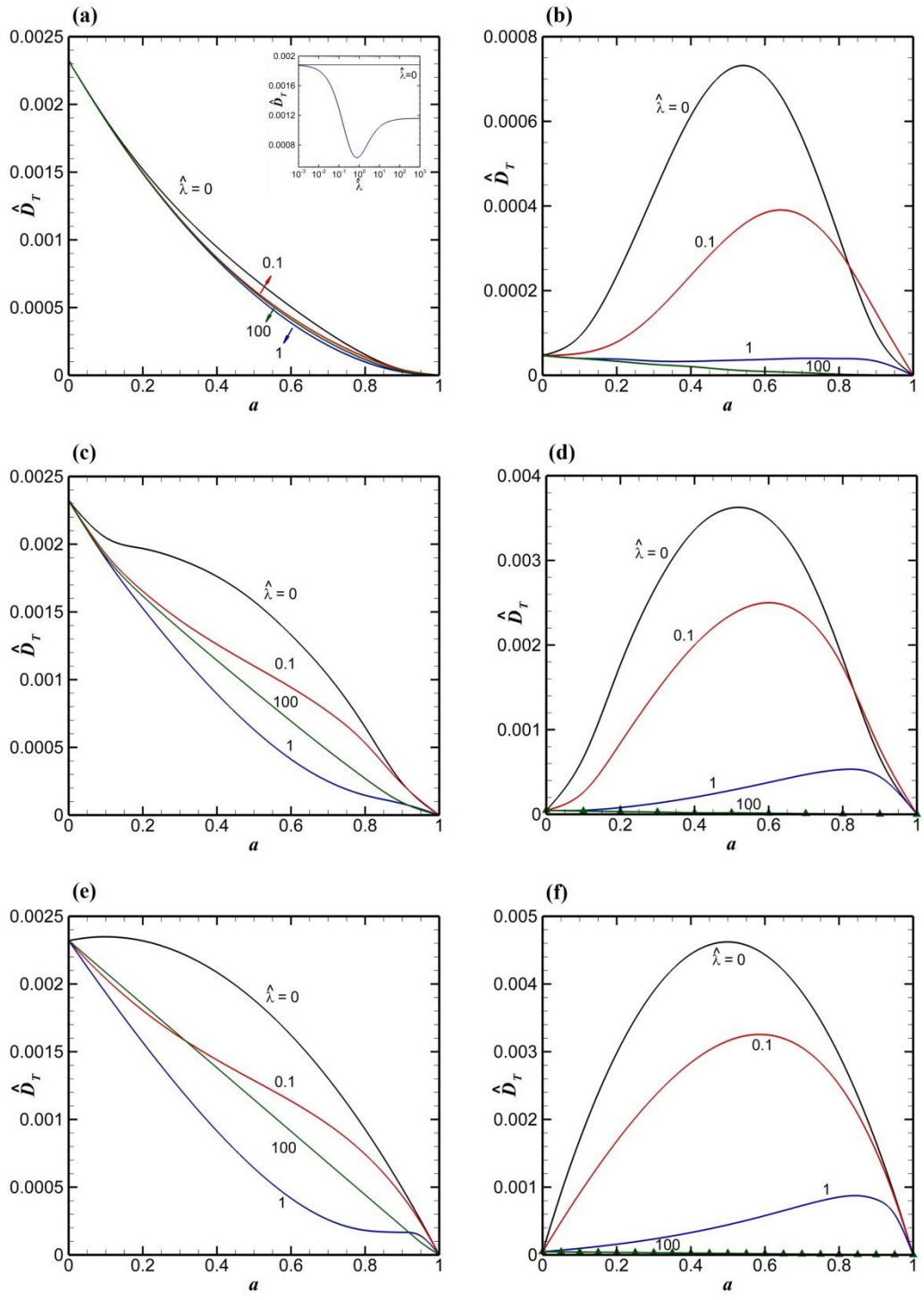

Figure 7. Dispersion coefficient $\hat{D}_T$ as a function of the slipping area fraction $0 \le a \le 1$, for $\hat{\zeta}_S = 0$, $\hat{\lambda} = 0,\ 0.1,\ 1,\ 100$, Pe $=10$. From left to right, $\hat{\kappa} = 10,\ 100$; from top to bottom, $\hat{l} = 1,\ 5,\ \infty$. **Inset 7(a):** dispersion coefficient $\hat{D}_T$ as a function of the intrinsic slip length $0.001 \le \hat{\lambda} \le 1000$, for $\hat{\zeta}_S = 0$, $a = 0.5$, $\hat{\kappa} = 10$, $\hat{l} = \infty$, Pe $=10$.

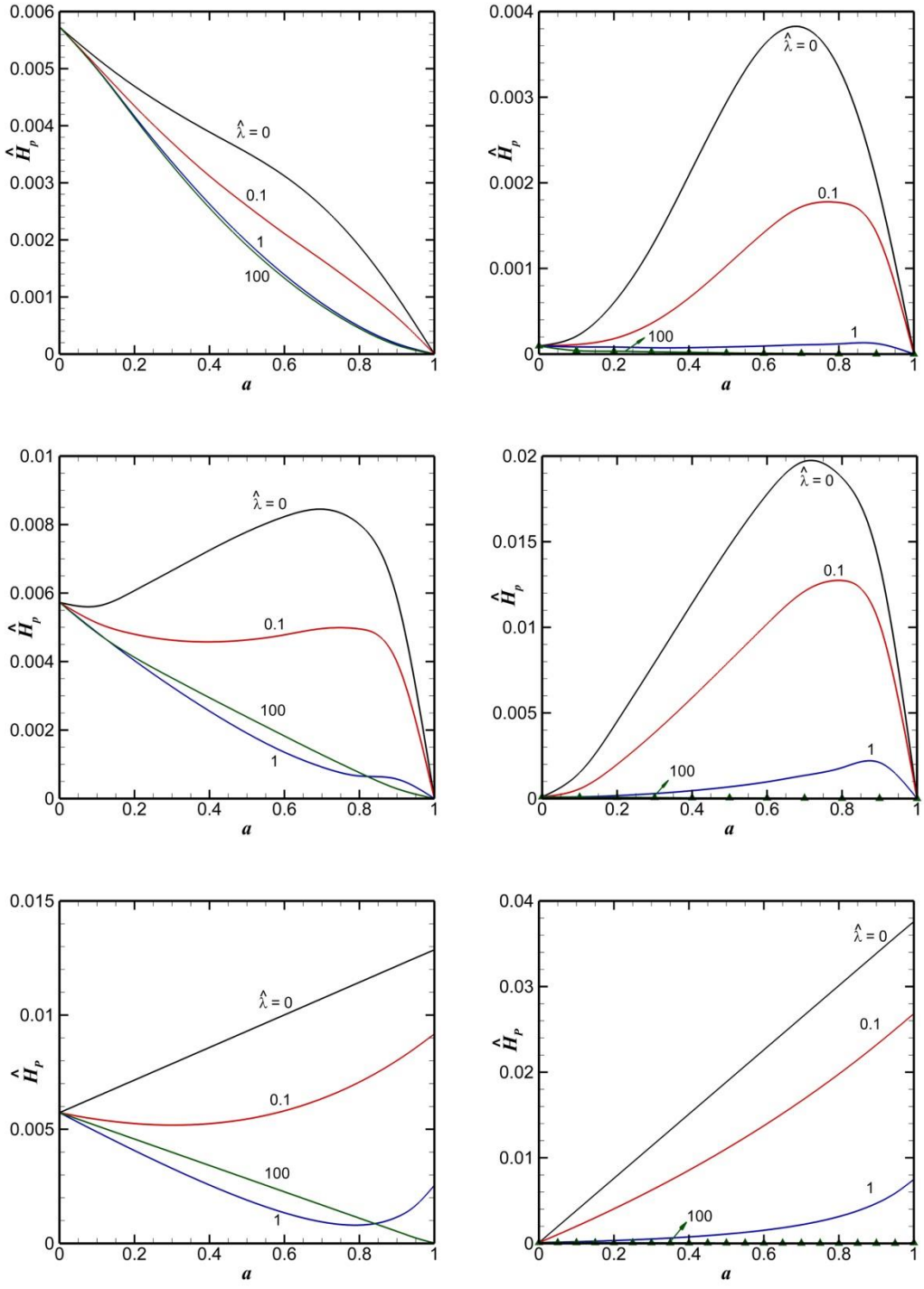

Figure 8. Plate height $\hat{H}_P$ as a function of the slipping area fraction $0 \le a \le 1$, for $\hat{\zeta}_S = 0$, $\hat{\lambda} = 0,\ 0.1,\ 1,\ 100$, Pe =10. From left to right, $\hat{\kappa} = 10,\ 100$; from top to bottom, $\hat{l} = 1,\ 5,\ \infty$.

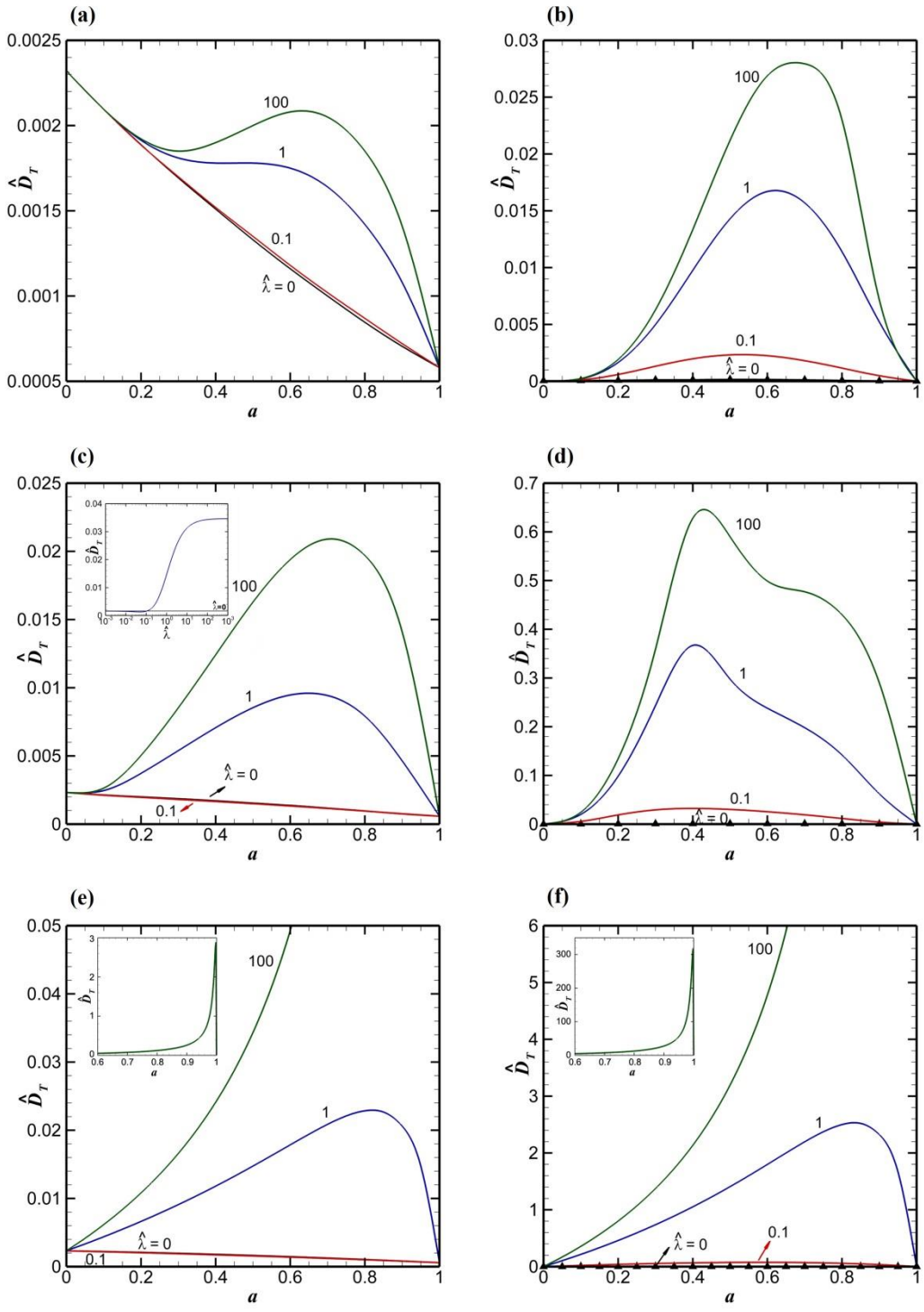

Figure 9. Dispersion coefficient $\hat{D}_T$ as a function of the slipping area fraction $0 \le a \le 1$, for $\hat{\zeta}_S = 0.5$, $\hat{\lambda} = 0,\ 0.1,\ 1,\ 100$, Pe $=10$. From left to right, $\hat{\kappa} = 10,\ 100$; from top to bottom, $\hat{l} = 1,\ 5,\ \infty$. **Inset 9(c):** dispersion coefficient $\hat{D}_T$ as a function of the intrinsic slip length $0.001 \le \hat{\lambda} \le 1000$, for $\hat{\zeta}_S = 0.5$, $a = 0.5$, $\hat{\kappa} = 10$, $\hat{l} = \infty$, Pe $=10$.

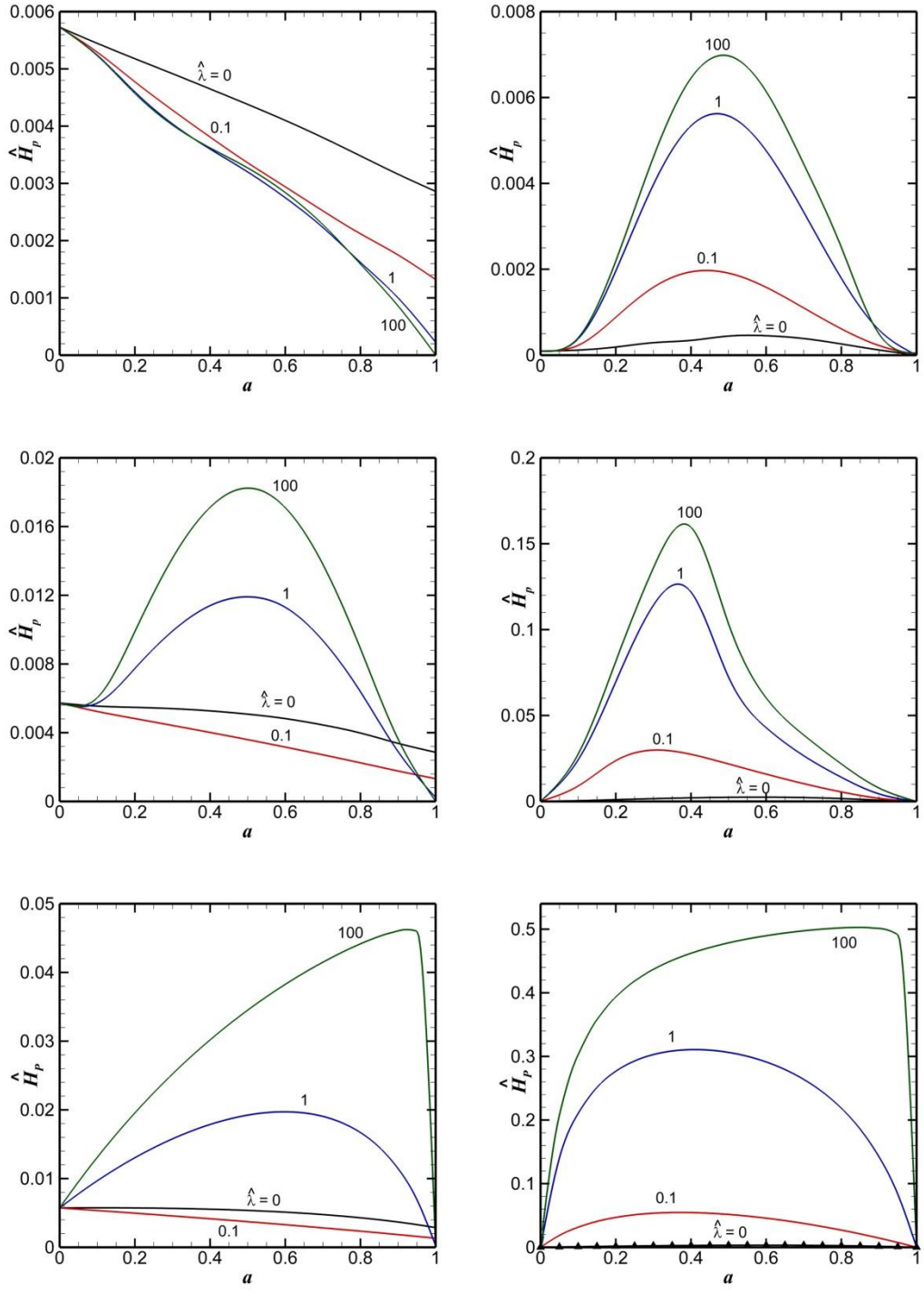

Figure 10. Plate height $\hat{H}_P$ as a function of the slipping area fraction $0 \le a \le 1$, for $\hat{\zeta}_S = 0.5$, $\hat{\lambda} = 0,\ 0.1,\ 1,\ 100$, Pe =10. From left to right, $\hat{\kappa} = 10,\ 100$; from top to bottom, $\hat{l} = 1,\ 5,\ \infty$.

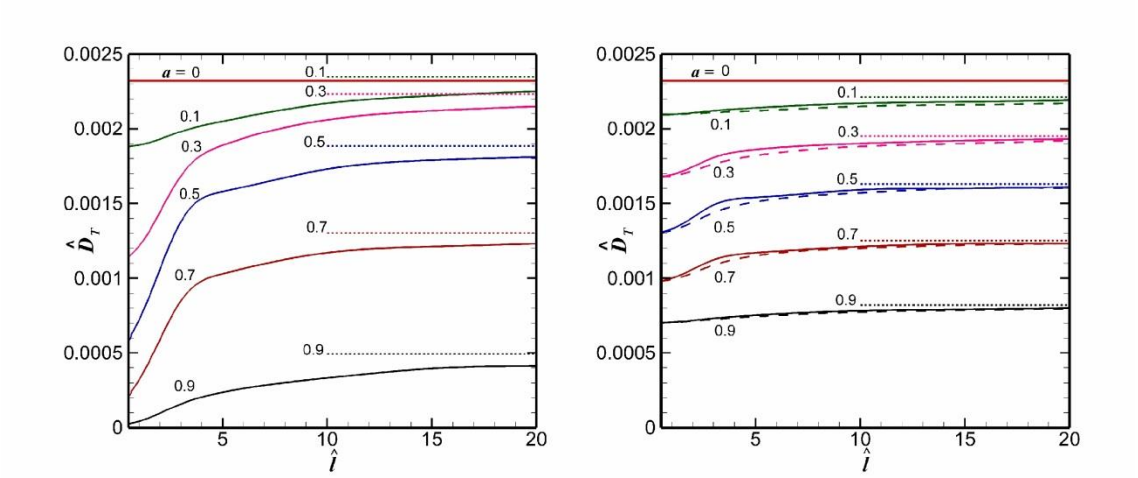

Figure 11. Dispersion coefficient $\hat{D}_T$ as a function of the period length $\hat{l}$, for $\hat{\lambda}=0$, $\hat{\kappa}=10$, $a=0,\ 0.1,\ 0.5,\ 0.9$, and (a) $\hat{\zeta}_S=0$, (b) $\hat{\zeta}_S=0.5$. The solid lines are for $\mathrm{Pe}=10$, while the dashed lines, in (b) only, are for $\mathrm{Pe}=20$. The solid lines are numerical results calculated from COMSOL, while the dotted lines are the long-wave limits calculated using equation (32).

Table 1. Error by the lubrication approximation

$\hat{D}_T$ ($\hat{l}=20$)	**Long-Wave Limit**	**Numerical Result**	**Error (100%)**
No-slip	0.0022113	0.002180	1.4
Par-slip	0.0043786	0.003729	17.4
Per-slip	0.0061638	0.005031	22.5
	eq. (32)	**comsol**	**|lw-nr|/nr**

*No-slip: $\hat{\lambda}=0$ Par-slip: $\hat{\lambda}=1$ Per-slip: $\hat{\lambda}=100$

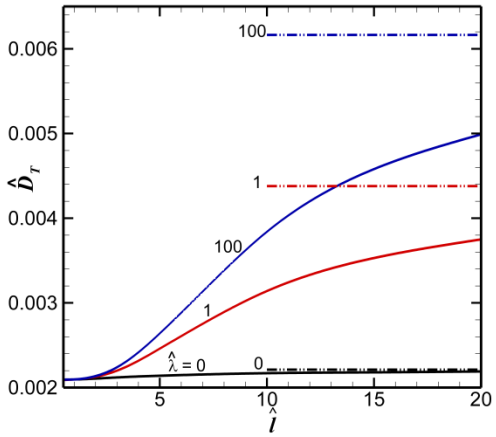

Figure 12. Dispersion coefficient $\hat{D}_T$ as a function of the period length $\hat{l}$, for $a=0.1$, $\hat{\zeta}_S=0.5$, $\hat{\kappa}=10$, $\mathrm{Pe}=10$, and $\hat{\lambda}=0,\ 1,\ 100$. The solid lines are numerical results calculated from COMSOL, while the dotted lines are the long-wave limits calculated using equation (32).